Band-gap measurements of direct and indirect semiconductors using monochromated electrons

Lin Gu,[1,*] Vesna Srot,[1] Wilfried Sigle,[1] Christoph Koch,[1] Peter van Aken,[1] Ferdinand Scholz,[2] Sarad B. Thapa,[2] Christoph Kirchner,[2] Michael Jetter,[3] and Manfred Rühle[1]

[1]*Max-Planck Institute for Metals Research, Heisenbergstrasse 3, D-70569 Stuttgart, Germany*

[2]*Institute of Optoelectronics, University of Ulm, Albert-Einstein-Allee 45, D-89069 Ulm, Germany*

[3]*Institut für Strahlenphysik, University of Stuttgart, D-70569 Stuttgart, Germany*

(Received 11 December 2006; revised manuscript received 23 February 2007; published 23 May 2007)

With the development of monochromators for transmission electron microscopes, valence electron-energy-loss spectroscopy (VEELS) has become a powerful technique to study the band structure of materials with high spatial resolution. However, artifacts such as Cerenkov radiation pose a limit for interpretation of the low-loss spectra. In order to reveal the exact band-gap onset using the VEELS method, semiconductors with direct and indirect band-gap transitions have to be treated differently. For direct semiconductors, spectra acquired at thin regions can efficiently minimize the Cerenkov effects. Examples of hexagonal GaN (*h*-GaN) spectra acquired at different thickness showed that a correct band-gap onset value can be obtained for sample thicknesses up to 0.5 t/λ. In addition, ω-q maps acquired at different specimen thicknesses confirm the thickness dependency of Cerenkov losses. For indirect semiconductors, the correct band-gap onset can be obtained in the dark-field mode when the required momentum transfer for indirect transition is satisfied. Dark-field VEEL spectroscopy using a star-shaped entrance aperture provides a way of removing Cerenkov effects in diffraction mode. Examples of Si spectra acquired by displacing the objective aperture revealed the exact indirect transition gap E_g of 1.1 eV.

DOI: 10.1103/PhysRevB.75.195214 PACS number(s): 71.20.−b, 87.64.Ee, 41.60.Bq

I. INTRODUCTION

Low-loss electron-energy-loss spectroscopy (EELS) investigates the energy-loss range of less than 50 eV. This energy range contains a wealth of fundamental material information including plasmon excitations and interband and intraband transitions. One of the most important parameters for semiconductors, the band-gap value, also occurs in this energy range. Traditionally, semiconductor band gaps are measured by optical methods which have high energy resolution (~2 meV) but poor spatial resolution (~0.2 μm). This spatial resolution is clearly not sufficient for measuring band gaps in modern nanostructured devices with structures in the nanometer range. Hence there is a demand for both high energy and high spatial resolution techniques for band-gap measurements.

It is not until recently that the valence electron-energy-loss spectroscopy has been used for band-gap measurements of materials with high spatial resolution in transmission electron microscopes (TEM). Reasons for this late approach in comparison to the core-loss EEL spectroscopy are mainly attributed to the limited energy resolution and the stability of the electron optics. In a standard TEM, the energy spread of the electron source, spectrometer aberrations, imperfections of parallel EELS detectors, and the instabilities of electrical and mechanical components of the whole TEM/EELS system are the major limitations to implement the VEELS techniques.[1]

The energy spread of the electron source is one of the most important aspects to be improved. An electron microscope equipped with a thermally assisted Schottky field-emission source normally has an energy resolution of about 0.8 eV under normal operation conditions. However, because of the low intensity of interband transitions the tail in the zero-loss peak makes it difficult to separate the signal from the background up to energy losses of 5 eV. Cold field-emission electron sources provide an energy resolution down to about 0.3 eV with the zero-loss tail extending to about 3 eV.[2] However, the asymmetrical nature of the zero-loss peak, which is caused by the emission process, complicates the removal of the zero-loss peak.[3,4] Recently, several types of monochromators were developed and advantages of using monochromated electron-energy-loss spectroscopy were also demonstrated.[4–13] Despite this technological breakthrough, there are still restrictions for band-gap measurements using VEELS in terms of spatial resolution and precise band-gap value measurements. The ultimate spatial resolution obtainable in an energy-filtered image or a STEM spectrum image is limited by the inelastic delocalization phenomenon, especially for the energy-loss range close to the semiconductor band-gap region.[14–16] In addition, Cerenkov radiation and surface effects impose artifacts on band-gap measurements for a wide range of semiconductors and insulators.[17–19]

In this paper, semiconductors with direct and indirect band-gap transitions were treated differently. For direct band-gap semiconductors, spectra acquired at thin regions can efficiently minimize the Cerenkov effects. For indirect band-gap semiconductors, the correct band-gap onset can be obtained in the dark-field mode by blocking the Cerenkov losses while maintaining the required momentum transfer.

II. EXPERIMENTAL DETAILS

The *h*-GaN thin film was grown on [0001] sapphire by metal-organic chemical vapor deposition (MOCVD). The total thickness of GaN was approximately 2 μm. Cross-sectional GaN and Si TEM specimens were prepared by double dimpling with final thinning using a precision-ion-

 ©2007 The American Physical Society

polishing system (PIPS, Gatan, Pleasanton, CA). The ion polish was carried out at 3.8 keV energy without liquid nitrogen cooling and followed by a 1.8 keV cleaning process. For TEM observation, GaN, Si, and diamond specimens were aligned on [1-100], [110] and [100] zone axes, respectively.

All spectra within this paper were acquired using a Zeiss Libra 200FE transmission electron microscope (operated at an accelerating voltage of 200 keV) equipped with an electrostatic omega-type monochromator (CEOS GmbH),[20] an in-column corrected 90° energy-filter, and a $2k \times 2k$ charge coupled device (CCD) camera (Gatan, Pleasanton, CA). The energy resolution of the microscope is 135 meV under normal operation conditions (acquisition time $\leqslant 1$ s), whereas for dark-field spectroscopy (see Sec. III B) the energy resolution degrades to about 0.5 eV because of the long exposure time of 30 min. All the EEL spectra obtained in image mode were acquired at a dispersion of 0.032 eV/channel with a collection angle of 3 mrad. For the ω-q maps the specimen was raised above the eucentric position in image mode with spot illumination[21] and the same dispersion of 0.032 eV/channel was used. Zero-loss deconvolution was applied for GaN spectra using the Richardson-Lucy method (DeConvEELS v2.0, HREM-Research, Higashimastuyama, Japan).[22] During the deconvolution process a smoothing width of 0.2 eV was used in order to prevent the amplification of noise by the deconvolution algorithm. The iteration cycles were constrained manually to prevent apparent artifacts. In the case of the Si spectra, zero-loss extraction was applied using the reflected-tail model implemented in DigitalMicrograph version 3.10.0 (Gatan, Pleasanton, CA).

III. RESULTS AND DISCUSSIONS

A. Direct semiconductors

The semiconductor band gap refers to the energy difference between the top of the valence band and the bottom of the conduction band. A direct band gap means that the minimum of the conduction band lies directly above the maximum of the valence band in momentum space. Therefore no momentum transfer is required to launch the electron from the valence band into the conduction band. Peaks in the VEEL spectrum are expected at energy losses where the joint density-of-states (JDOS) exhibits maxima, i.e., at positions of vanishing slope of the bands of initial and final states in the energy-momentum diagram.[23] In semiconductors with indirect band gap, such as silicon or diamond, changes in both energy and momentum are involved in the excitation process across the band gap.

h-GaN is a direct band-gap semiconductor for applications in high-temperature and high-power microelectronics as well as in light-emitting devices. The optical properties and the band-gap value of *h*-GaN have been extensively studied in the past.[24–26] From optical absorption data, the band gap of *h*-GaN was determined to be 3.43 eV.[27] In this study, the *h*-GaN band gap was measured at liquid nitrogen temperature and the onset value was determined to be 3.3 eV using the deconvolution method. One possible reason for this low band-gap value could be attributed to crystal defects

TABLE I. Measured band-gap onset values using different spectrum processing techniques(ZLP is zero-loss peak).

Methods	Onset values (eV)	References
Fourier-log deconvolution Fit of power-law function to the onset	3.3	10
Fourier-ratio deconvolution	3.3	3
Power-law fit to ZLP Fit of Lorentzian peaks to first derivative	3.4	29, 30
Visual determination of the changing slope at the onset	3.4	4
Mirroring left tail of ZLP to the right tail Subtraction of the mirrored tail defining the inflection point as the onset	3.5	26

which always shift the onset to lower energies.[28] However, the energy onset for interband transitions may also be influenced by the spectrum processing technique. In the literature (Refs. 2–4, 10, 26, and 29–33) various techniques were applied to retrieve the onset energy. We applied these techniques to one of our experimental spectra and the onset energies are listed in Table I. The values range from 3.3 to 3.5 eV which shows that the systematic error introduced by the data processing is about ±0.1 eV. For consistency of the paper, the following discussions on direct semiconductors are all based on the deconvolution method.

The original VEEL spectrum is shown in Fig. 1(a). Zero-loss deconvolution was applied to reveal the exact band-gap onset which is shown in Fig. 1(b). From this deconvoluted VEEL spectrum, not only the band-gap onset value, but also plenty of information concerning interband transitions at higher energy is obtained with an excellent signal-to-noise ratio. All peaks presented in Fig. 1(b) can be attributed to direct interband transitions between states of high density which are so-called critical points[23] (see also Fig. 3 below).

One of the major limitations for VEELS studies of semiconductor band gaps is Cerenkov radiation. Cerenkov radiation is emitted when the electron velocity v exceeds the speed of light (or more precisely, its phase velocity) in the medium through which it is moving. The electric field surrounding a moving charged particle displaces and polarizes the electrons in the atoms of the medium it travels through. When the polarized medium restores itself after the electron has passed, virtual photons are emitted. If the beam electron moves faster than the phase velocity of light in this medium, i.e., if the real part of the dielectric constant $\varepsilon_1(E) > c^2/v^2$, the emitted photons are left behind by the fast moving electron, and, for a certain direction of propagation, interfere constructively, leading to the emission of light at the cost of energy loss to the beam electron.[17,34] From the above criterion, it is obvious that Cerenkov radiation can be avoided by lowering the speed of the electrons, i.e., by decreasing the high voltage. Table II gives examples of some typical semiconductors with their refractive indices[35–41] and the corresponding critical high voltage below which Cerenkov radiation does not occur. For certain semiconductors such as AlN,

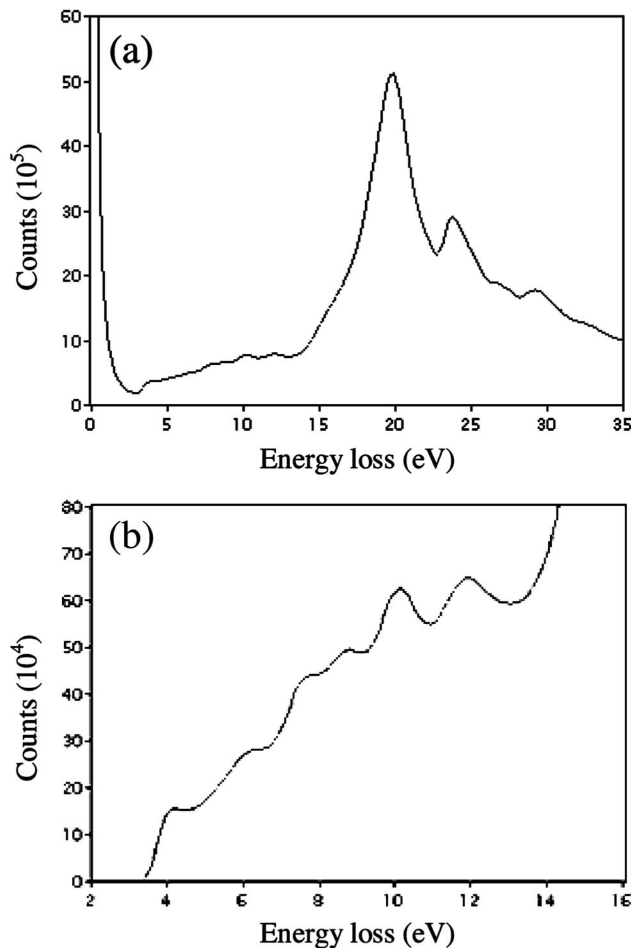

FIG. 1. Low-loss EELS spectra of *h*-GaN: (a) raw spectrum and (b) zero-loss deconvoluted spectrum showing the band-gap onset and interband transitions. Peaks originate from critical points in the band structure.

it may be feasible to reduce the high tension to avoid Cerenkov losses, however, at the cost of degrading the microscope performance. Note that the refractive indices are energy dependent, the critical high voltages for AlN and GaN calculated in Table II need to be further decreased at higher photon energies.[35,42] For semiconductors with high refractive index, the required low acceleration voltages are impractical, therefore alternative methods have to be found.

For specimens which are not too thin, so that the surface effects can be neglected, the double-differential scattering cross section for volume losses including Cerenkov radiation is described as[18,43,44]

$$\frac{d^2\sigma^{\text{Volume}}}{d\Omega\, dE} = \frac{\text{Im}(-1/\varepsilon)}{a_0 m_0 \pi^2 v^2 n_a} \frac{\theta^2 + \theta_E^2[(\varepsilon_1 v^2/c^2 - 1)^2 + \varepsilon_2^2 v^4/c^4]}{[\theta^2 - \theta_E^2(\varepsilon_1 v^2/c^2 - 1)]^2 + \theta_E^4 \varepsilon_2^2 v^4/c^4}, \tag{1}$$

where $a_0 = \varepsilon_0 \hbar^2 / m_0 e^2 \pi = 0.529 \times 10^{-10}$ m is the first Bohr radius, n_a is the number of atoms per unit volume, and ε_1 and ε_2 are the real and imaginary part of the dielectric function $(\varepsilon = \varepsilon_1 + i\varepsilon_2)$. The full equation, including surface effects, was given by Kröger.[44] Since the classical nonrelativistic Lorentzian term is replaced by a more complicated function in Eq. (1), the denominator can become small at specific scattering angles, which results in a large cross section even below the band gap where ε_2 is very small. From Eq. (1) it can be derived that $\frac{d^2\sigma^{\text{Volume}}}{d\Omega dE} \propto D$ where D is the specimen thickness.[19,44] This means that in the absence of surfaces both interband transitions [included in $\text{Im}(-1/\varepsilon)$] and Cerenkov losses increase with the thickness of the specimen. This is not true anymore if the specimen thickness is of a similar magnitude as the wavelength of the emitted Cerenkov light, which is the case in thin TEM specimens. Under such conditions the surfaces damp the Cerenkov losses. To summarize, in thick specimens the Cerenkov cross section can be of similar magnitude as the cross section for interband transitions, whereas Cerenkov losses are less prominent in thinner specimen areas.[44] Strong Cerenkov losses can lead to an apparent shift of the band gap towards lower energy.[19,44]

Two GaN VEEL spectra acquired at different thicknesses with $t/\lambda = 0.4$ (thin) and 1.6 (thick) are shown in Fig. 2(a). In this expression, t is the sample thickness and λ is the mean free path of inelastic scattering. Under the experimental conditions described earlier, the inelastic mean free path for GaN was estimated to be about 140 nm.[45] Since 200 keV electrons have a speed of about $0.7c$, they suffer from Cerenkov losses in GaN which has a refractive index of about 2.4 (Ref. 36) (at 532 nm). The spectrum in Fig. 2(a) from the thin region shows the correct band-gap value of 3.3 eV. This shows that for this specimen thickness the damping of the Cerenkov light is so strong that a measurement of the direct band-gap onset is possible. A systematic study of the appar-

TABLE II. Refractive indices of some semiconductors and corresponding critical high voltages below which Cerenkov radiation does not occur.

Semiconductors	Refractive indices (at 300 K)	Remarks	Critical high voltage (keV)
AlN (wurtzite)	2.1	At ≈2.1 eV (Ref. 35)	70
h-GaN (wurtzite)	2.4	At ≈2.3 eV (Ref. 36)	51
Diamond	2.7	At ≈5.5 eV (Ref. 37)	39
Silicon	3.4	At ≈1.2 eV (Refs. 38 and 39)	24
GaAs	3.6	At ≈1.4 eV (Ref. 40)	21
Germanium	4.2	At ≈0.8 eV (Ref. 41)	15

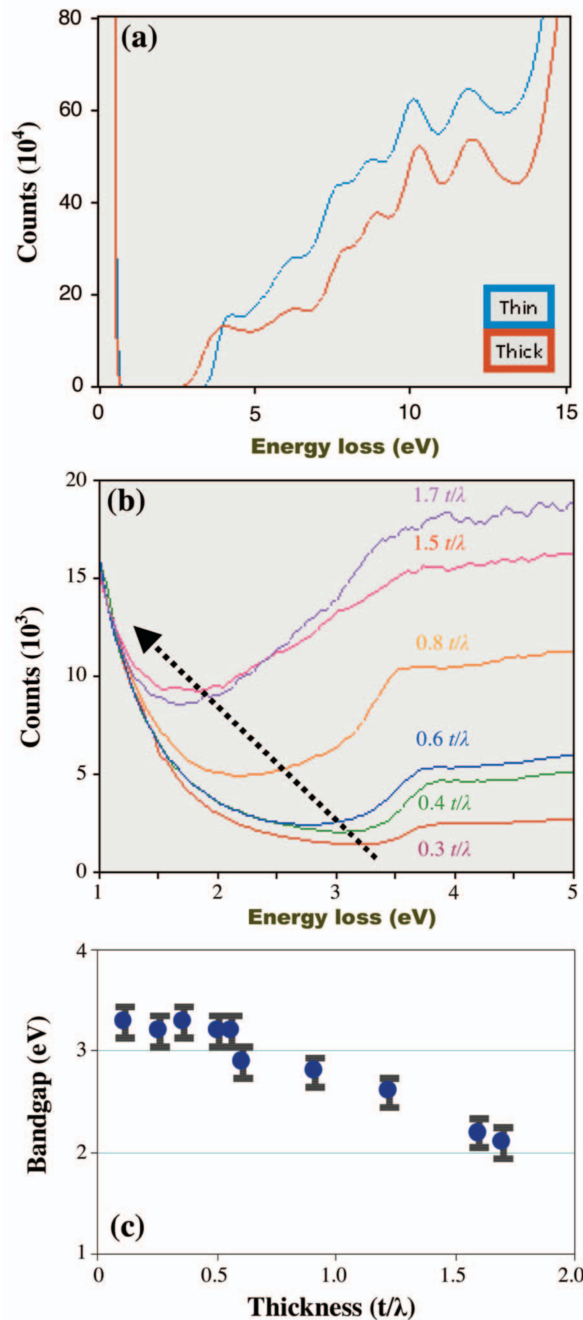

FIG. 2. (Color) (a) h-GaN VEEL spectra measured at different specimen thicknesses; (b) systematic shift of the apparent band gap to lower energies with increasing sample thickness; and (c) plot of apparent band gap versus sample thickness showing the true band-gap value below 0.5 t/λ.

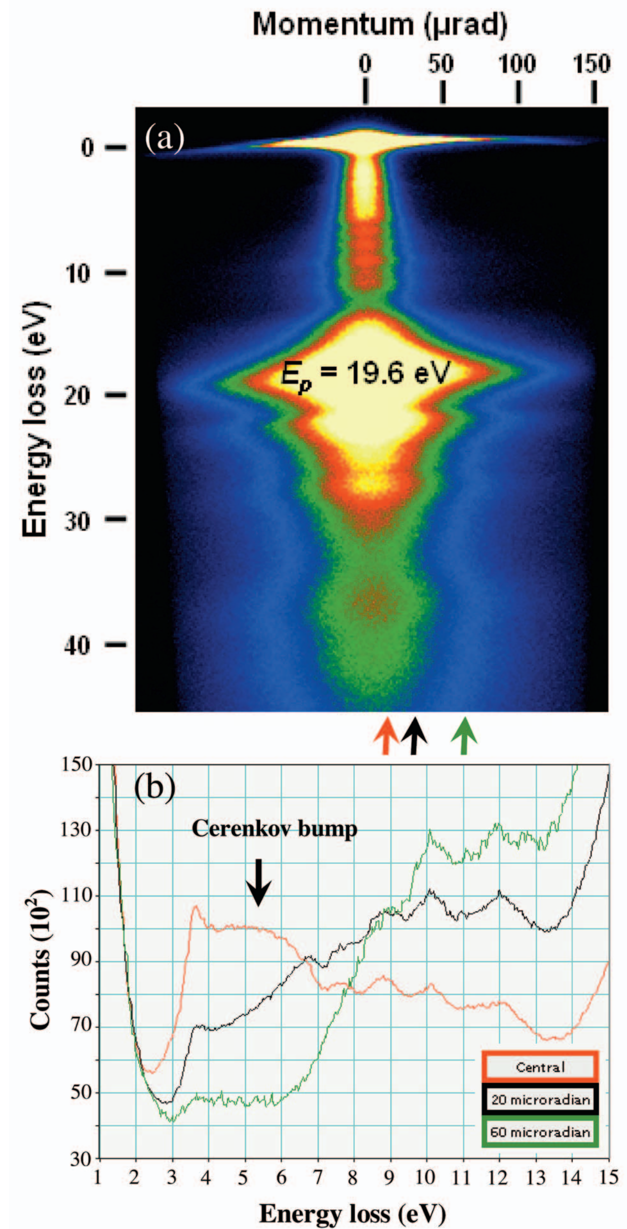

FIG. 3. (Color) (a) ω-q map of h-GaN at a thick region with strong Cerenkov losses and (b) line profiles extracted at different q values with a linewidth of about 5 μrad. The energy loss of Cerenkov radiation has a narrow angular distribution.

ent onset of interband transitions for specimen thicknesses between 0.3 and 1.7 inelastic mean free paths is shown in Fig. 2(b). Similar to the results shown in Refs. 19 and 44, a systematic shift of the onset is found with increasing thickness. The observed band-gap onset shifts from 3.3 to about 2.0 eV. The thickness-dependent onset energies are shown in Fig. 2(c). Error bars are based on the energy resolution of the microscope. It was found that the correct h-GaN band-gap onset can be obtained for specimen thicknesses up to 0.5 t/λ. Above this value interpretation of VEELS measurements becomes increasingly complicated by the Cerenkov losses.

The angular distribution of electrons which have suffered Cerenkov losses (hereafter called "Cerenkov electrons") is not readily visible under normal TEM operation conditions. This is because those Cerenkov electrons are confined to a very narrow angular range close to the scattering angle $\theta = \theta_E(\varepsilon_1 v^2/c^2 - 1)$ [see Eq. (1)]. Therefore it is necessary to use fairly large camera lengths.[46,47] Figure 3(a) shows the ω-q map of h-GaN acquired at a rather thick region. The interband transitions and volume plasmon are clearly observed. These interband transitions are supposed to be direct transitions[24] since no momentum transfer q perpendicular to

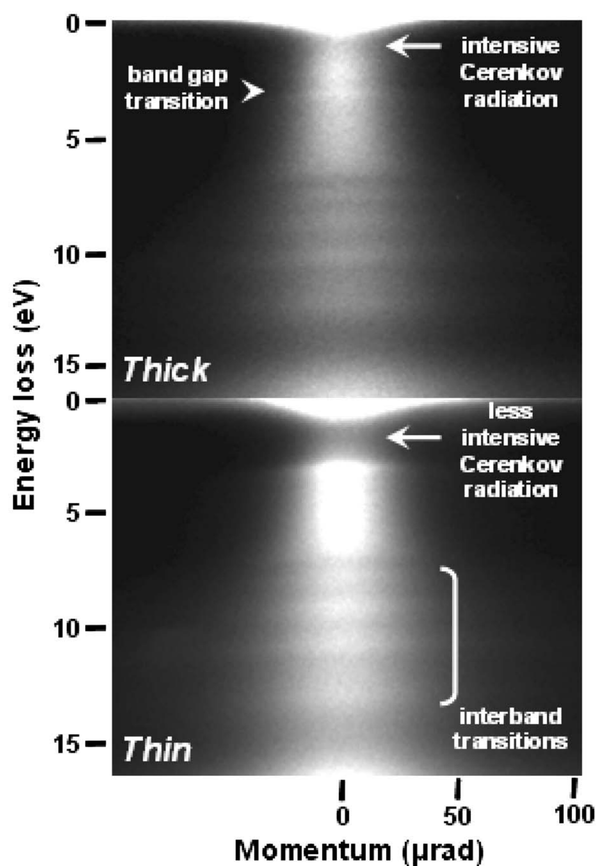

FIG. 4. ω-q maps of h-GaN acquired at different thicknesses. Cerenkov losses are less pronounced at thin regions.

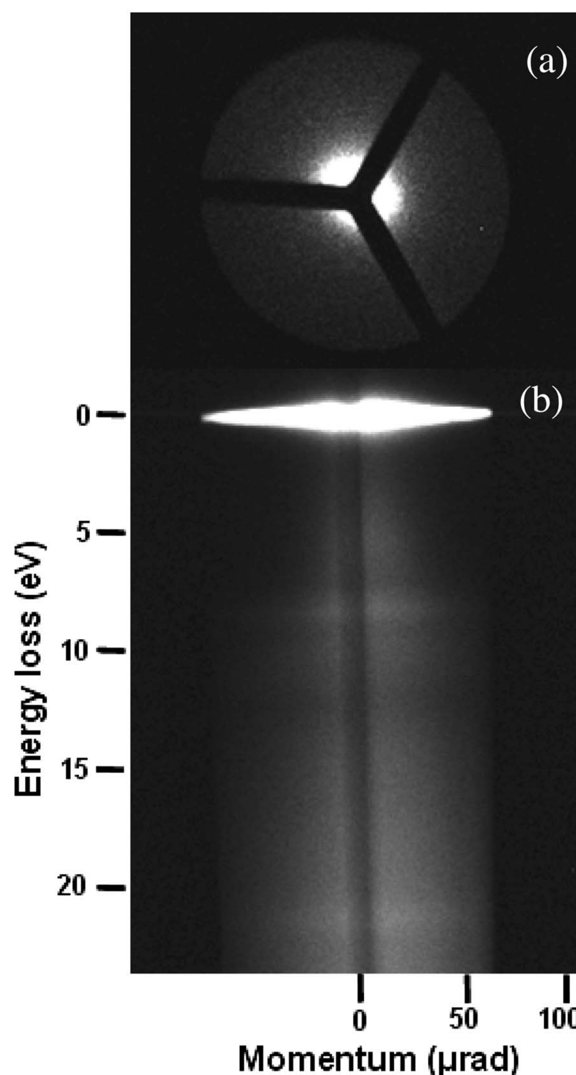

FIG. 5. Star-shaped filter-entrance aperture used for dark-field VEEL spectroscopy: (a) Image of the aperture in diffraction mode and (b) spectrum obtained by using this aperture.

the direction of the incident beam of electrons is involved. In the band-gap region, intensive Cerenkov radiation is observed which overlaps with the band-gap transition at 3.3 eV, leading to the described downwards shift of the apparent onset energy. Since most VEELS measurements only reflect this apparent onset energy which includes both genuine band-gap transitions and artifacts from Cerenkov radiation, it is very important to reduce the specimen thickness for less Cerenkov losses. Figure 3(b) shows line profiles extracted from different q values [marked by arrows in Fig. 3(a)] using a linewidth of about $5\,\mu$rad. The spectral intensities were normalized in the energy-loss range from 1 to 2 eV. An intensive energy-loss peak due to Cerenkov radiation is observed. Because of the small angular range of "Cerenkov electrons" this peak is much stronger close to $q=0$ than for $|q|>0$. From Fig. 3(b) h-GaN VEEL spectra show significant Cerenkov contribution when collected with a collection aperture of 20 μrad. For larger collection angles the relative Cerenkov intensity becomes smaller.

ω-q maps of h-GaN at different thicknesses are shown in Fig. 4. Comparison of the spectra shows great similarity for the plasmon losses as well as for the interband transitions which were also revealed in Fig. 2(a). However, the more intensive Cerenkov losses in thick regions overlap severely with the band-gap transitions. This clearly confirms that the apparent shift of the band gap towards lower energies at increasing thickness is due to Cerenkov losses.

The necessity of using thin specimen areas to obtain true band-gap values implicates the danger of local nonstoichiometry of the specimen due to specimen preparation artifacts. In addition, excitation of surface plasmons can become important. Although these seemed to be negligible effects in our measurements, one has to keep in mind their possible influence.[48,49]

B. Indirect semiconductors

Indirect band-gap semiconductors do not have the lowest conduction band energy at the Γ point. Therefore the fast electron has to transfer momentum to an electron in the valence band in order to excite it into the conduction band. This also implies that the cross section for interband transitions is lower than in the case of direct semiconductors which, in turn, makes Cerenkov losses more prominent. Examples of Si VEEL spectra have shown the difficulties in interpreting the low-loss data due to strong Cerenkov radiation

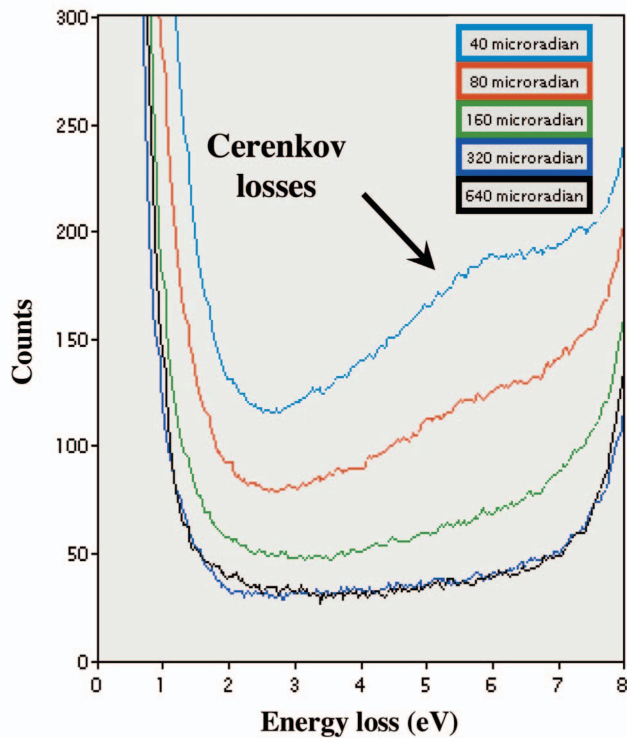

FIG. 6. (Color) Low-loss diamond spectra acquired with different collection angles showing the blocking of Cerenkov losses.

losses.[4,19,50] Therefore alternative ways have to be undertaken for accurate measurements of the band-gap value.

Since "Cerenkov electrons" have a very narrow angular distribution, and indirect semiconductors normally require a large momentum transfer $q_\perp$ for the band-gap transition,[51] we suggest "dark-field VEEL spectroscopy" for band-gap measurements of indirect semiconductors. Figure 5(a) shows the geometry of a star-shaped filter-entrance aperture which can efficiently suppress the collection of Cerenkov losses while permitting the high-angle indirect band-gap transitions. The corresponding diamond spectrum acquired in diffraction EELS mode in Fig. 5(b) shows dark contrast along the central region of the dispersion axis which is attributed to the presence of the aperture.

In comparison to other dark-field spectroscopy techniques, this aperture has certain advantages. For instance, although it is possible to exclude Cerenkov losses from VEEL spectra by using ω-q maps and integrating the high-angular range, the signal-to-noise ratio can be quite poor because of the limited dynamic range of the CCD and the intensive Cerenkov losses at small q. Moreover, displacing the objective aperture allows selecting the desired momentum transfer, however, the long acquisition time degrades the energy-resolution of the spectra due to potential microscope instabilities.

By varying the camera length, the angular range which is blocked by the aperture can be varied. As the camera length decreases, the angular width of the central (blocked) region increases. Figure 6 shows dark-field diamond VEEL spectra measured at different camera lengths. When the central range of the aperture is greater than the Cerenkov cone, Cerenkov

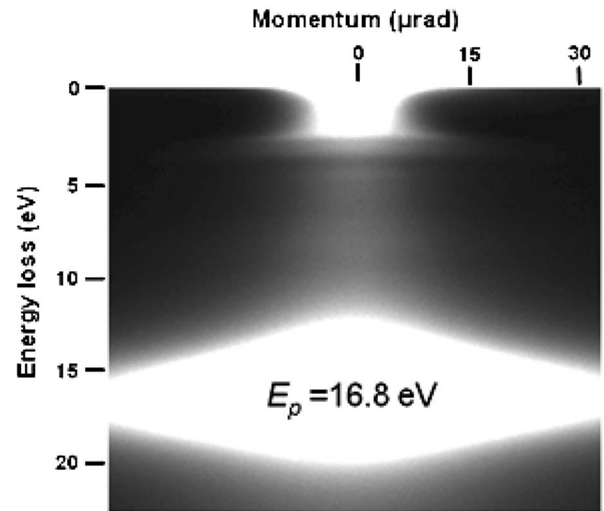

FIG. 7. ω-q map of Si showing Cerenkov losses across the band-gap region.

losses are blocked by the aperture. In our example this happens if the blocked angular range exceeds about 320 μrad. At larger camera lengths an intensive Cerenkov peak is observed. For example, in the case of blocking 40 μrad, the energy onset of Cerenkov radiation at about 2.5 eV is observed.

To perform dark-field VEEL spectroscopy on indirect semiconductors it is also possible to use a normal round filter entrance aperture in diffraction mode (or objective aperture in image mode). Since the double-differential cross section for inelastic scattering is proportional to both JDOS and the form factor,[51,52]

$$\frac{d^2\sigma}{d\Omega dE} \propto \left| \sum_{j=1}^{N} \langle f|\exp(iq \cdot r_j)|i\rangle \right|^2 \rho(E), \tag{2}$$

it is important to select an appreciable momentum range $q_\perp$ covering the desired indirect band-gap transitions. The ω-q map of Si aligned along the [110] zone axis [Fig. 7(a)] shows

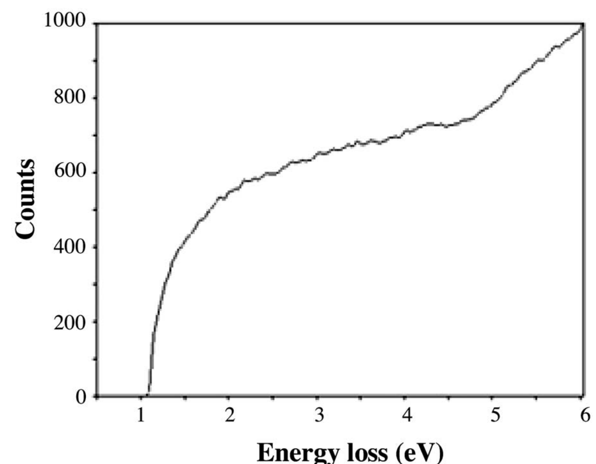

FIG. 8. Dark-field VEEL spectrum of Si showing the band-gap onset at 1.1 eV.

a significant amount of Cerenkov radiation losses which is responsible for the apparently thickness-dependent band-gap data.[19] By displacing the entrance aperture in diffraction mode along the Γ-X direction to a position approximately at the Brillouin zone boundary, the correct band-gap value of about 1.1 eV can be measured. This is shown in Fig. 8. However, in this mode, information about direct transitions such as $E_{\Gamma 1}$ (3.4 eV) and $E_{\Gamma 2}$ (4.2 eV) is lost. In order to reveal this information, careful removal of relativistic effects is required, e.g., by quantitative comparison with calculated Cerenkov spectra. Another drawback of this technique is the acquisition time, which requires a stable experimental environment both electronically and mechanically. Unfortunately, at present, this is available only in a few microscopes.

IV. CONCLUSIONS

VEELS band-gap measurements for direct and indirect semiconductors have been performed using monochromated electrons. Major limitations for low-loss EELS such as Cerenkov radiation losses were discussed and possible circumvention methods were proposed. For direct semiconductors, VEEL spectra acquired at thin regions can efficiently minimize the Cerenkov effects. For indirect semiconductors such as diamond, dark-field VEEL spectroscopy using a star-shaped entrance aperture showed restrained Cerenkov losses. Examples of Si spectra acquired by displacing the objective aperture revealed the exact indirect transition gap E_g of 1.1 eV. However, limitations of these methods still exist including surface effects for very thin specimens and long acquisition time for dark-field spectroscopy.

ACKNOWLEDGMENTS

The authors acknowledge financial support from the European Union under the Framework 6 program under a contract for an Integrated Infrastructure Initiative, Reference 026019 ESTEEM. The SESAM project has been funded jointly by the Deutsche Forschungsgemeinschaft, the Max Planck Society, and by the Ministry of Science and Education of the State of Baden-Württemberg.

---

*Corresponding author. Email address: gu@mf.mpg.de

[1] W. Sigle, Annu. Rev. Mater. Res. **35**, 239 (2005).
[2] P. E. Batson, K. L. Kavanagh, J. M. Woodall, and J. W. Mayer, Phys. Rev. Lett. **57**, 2729 (1986).
[3] B. Rafferty, S. J. Pennycook, and L. M. Brown, J. Electron Microsc. **49**, 517 (2000).
[4] K. Kimoto, G. Kothleitner, W. Grogger, Y. Matsui, and F. Hofer, Micron **36**, 185 (2005).
[5] M. Terauchi, M. Tanaka, K. Tsuno, and M. Ishida, J. Microsc. **194**, 203 (1999).
[6] P. C. Tiemeijer, Ultramicroscopy **78**, 53 (1999).
[7] F. Kahl and H. Rose, in *Proceedings of EUREM-12: The 12th European Congress on Electron Microscopy*, edited by L. Frank and F. Ciampor (Committee of European Societies of Microscopy, Brno, Czech Republic, 2000), p. 459.
[8] H. W. Mook and P. Kruit, Ultramicroscopy **81**, 129 (2000).
[9] M. Tanaka, M. Terauchi, K. Tsuda, K. Saitoh, M. Mukai, T. Tomita, K. Tsuno, M. Kersker, M. Naruse, and T. Honda, Microsc. Microanal. **8**, 68 (2002).
[10] R. Erni and N. D. Browning, Ultramicroscopy **104**, 176 (2005).
[11] C. Mitterbauer, G. Kothleitner, W. Grogger, H. Zandbergen, B. Freitag, P. Tiemeijer, and F. Hofer, Ultramicroscopy **96**, 469 (2003).
[12] M. Terauchi and M. Tanaka, Micron **30**, 371 (1999).
[13] A. S. Sefat, G. Amow, M. Y. Wu, G. A. Botton, and J. E. Greedan, J. Solid State Chem. **178**, 1008 (2005).
[14] A. Howie, J. Microsc. **117**, 11 (1979).
[15] D. A. Muller and J. Silcox, Ultramicroscopy **59**, 195 (1995).
[16] M. P. Oxley and L. J. Allen, Phys. Rev. B **57**, 3273 (2000).
[17] P. A. Cerenkov, Dokl. Akad. Nauk SSSR **2**, 451 (1934).
[18] C. von Festenberg and E. Kroeger, Phys. Lett. **26A**, 339 (1968).
[19] M. Stoeger-Pollach, H. Franco, P. Schattschneider, S. Lazar, B. Schaffer, W. Grogger, and H. W. Zandbergen, Micron **37**, 396 (2006).
[20] F. Kahl and H. Rose, in *Proceedings of EUREM-11: The 11th European Conference on Electron Microscopy*, edited by P. Hawkes (Committee of European Societies of Microscopy, Dublin, Ireland, 1996), p. 478.
[21] P. A. Midgley, Ultramicroscopy **76**, 91 (1999).
[22] DeConvEELS v2.0, HREM Research, Higashimastuyama, Japan.
[23] M. G. Bell and W. Y. Liang, Adv. Phys. **25**, 53 (1976).
[24] S. Bloom, G. Harbeke, E. Meier, and I. B. Ortenburger, Phys. Status Solidi B **66**, 161 (1974).
[25] V. Bougrov, M. E. Levinshtein, S. L. Rumyantsev, and A. Zubrilov, in *Properties of Advanced Semiconductor Materials GaN, AlN, InN, BN, SiC, SiGe*, edited by M. E. Levinshtein, S. L. Rumyantsev, and M. S. Shur (Wiley, New York, 2001).
[26] S. Lazar, G. A. Botton, M. Y. Wu, F. D. Tichelaar, and H. W. Zandbergen, Ultramicroscopy **96**, 535 (2003).
[27] W. Shan, J. W. Ager III, K. M. Yu, W. Walukiewicz, E. E. Haller, M. C. Martin, W. R. McKinney, and W. Yang, J. Appl. Phys. **85**, 8505 (1999).
[28] A. Gutierrez-Sosa, U. Bangert, A. J. Harvey, C. Fall, and R. Jones, Diamond Relat. Mater. **12**, 1108 (2003).
[29] R. Erni and N. D. Browning, Ultramicroscopy **107**, 267 (2007).
[30] P. Specht, J. C. Ho, X. Xu, R. Armitage, E. R. Weber, R. Erni, and C. Kisielowski, Solid State Commun. **135**, 340 (2005).
[31] S. Schamm and G. Zanchi, Ultramicroscopy **96**, 559 (2003).
[32] L. A. J. Garvie, P. Rez, J. R. Alvarez, and P. R. Buseck, Solid State Commun. **106**, 303 (1998).
[33] A. Gutierrez-Sosa, U. Bangert, A. J. Harvey, C. J. Fall, R. Jones, P. R. Briddon, and M. I. Heggie, Phys. Rev. B **66**, 035302 (2002).
[34] I. M. Frank and I. Tamm, Dokl. Akad. Nauk SSSR **14**, 109 (1937).
[35] G. M. Laws, E. C. Larkins, I. Harrison, C. Molloy, and D. Somerford, J. Appl. Phys. **89**, 1108 (2001).
[36] N. A. Sanford, L. H. Robins, A. V. Davydov, A. Shapiro,

D. V. Tsvetkov, A. V. Dmitriev, S. Keller, U. K. Mishra, and S. P. DenBaars, J. Appl. Phys. **94**, 2980 (2003).
[37] W. C. Walker and J. Osantowski, Phys. Rev. **134**, A153 (1964).
[38] H. R. Philipp and E. A. Taft, Phys. Rev. **120**, 37 (1960).
[39] C. Salzberg and J. Villa, J. Opt. Soc. Am. **47**, 244 (1957).
[40] J. S. Blakemore, J. Appl. Phys. **53**, R123 (1982).
[41] H. R. Philipp and E. A. Taft, Phys. Rev. **113**, 1002 (1959).
[42] G. Yu, G. Wang, H. Ishikawa, M. Umeno, T. Soga, T. Egawa, J. Watanabe, and T. Jimbo, Appl. Phys. Lett. **70**, 3209 (1997).
[43] E. Kroeger, Z. Phys. **216**, 115 (1968).
[44] C. von Festenberg, Z. Phys. **214**, 464 (1968).
[45] R. F. Egerton and S. C. Cheng, Ultramicroscopy **21**, 231 (1987).
[46] R. B. Pettit, J. Silcox, and R. Vincent, Phys. Rev. B **11**, 3116 (1975).
[47] C. H. Chen, J. Silcox, and R. Vincent, Phys. Rev. B **12**, 64 (1975).
[48] C. von Festenberg, Z. Phys. **227**, 453 (1969).
[49] F. J. Garcia de Abajo, A. Rivacoba, N. Zabala, and N. Yamamoto, Phys. Rev. B **69**, 155420 (2004).
[50] H. Kohno, T. Mabuchi, S. Takeda, M. Kohyama, M. Terauchi, and M. Tanaka, J. Electron Microsc. **47**, 311 (1998).
[51] R. Rafferty and L. M. Brown, Phys. Rev. B **58**, 10326 (1998).
[52] M. Inokuti, Rev. Mod. Phys. **43**, 297 (1971).